A model of the pressure dependence of the enantioselectivity of *Candida rugosa* lipase towards (±)-menthol

Ulrich H. M. Kahlow, Rolf D. Schmid, Jürgen Pleiss*

Institute of Technical Biochemistry, University of Stuttgart, Allmandring 31, D-70569 Stuttgart, Germany

47 manuscript pages

0 supplementing material pages

4 tables

17 figures (numbered 1-10, including figures 5A and 5B, 8A to 8D, and 10A to 10D)

CD-ROM included

Environment: MS-Windows NT4.0, MS-Word'97, Origin 5.0, Excel'97

To whom correspondence should be addressed:

Dr. Jürgen Pleiss

Institute of Technical Biochemistry

University of Stuttgart

Allmandring 31

70561 Stuttgart

Germany

Phone: +49/(0)711/685-3191

Fax: +49/(0)711/685-3196

Email: itbjpl@po.uni-stuttgart.de

Abstract

Transesterification of (±)-menthol using propionic acid anhydride and *Candida rugosa* lipase was performed in chloroform and water at different pressures (1, 10, 50, and 100 bar) to study the pressure dependence of enantioselectivity E. As a result, E significantly decreased with increasing pressure from E=55 (1 bar) to E=47 (10 bar), E=37 (50 bar), and E=9 (100 bar).

In order to rationalize the experimental findings, molecular dynamics simulations of *Candida rugosa* lipase were carried out. Analyzing the lipase geometry at 1, 10, 50, and 100 bar revealed a cavity in the *Candida rugosa* lipase. The cavity leads from a position on the surface distinct from the substrate binding site to the core towards the active site and is limited by F415 and the catalytic H449. In the crystal structure of the *Candida rugosa* lipase, this cavity is filled with 6 water molecules. The number of water molecules in this cavity gradually increased with increasing pressure: 6 molecules in the simulation at 1 bar, 10 molecules at 10 bar, 12 molecules at 50 bar, and 13 molecules at 100 bar. Likewise, the volume of the cavity progressively increased from about 1864 Å³ in the simulation at 1 bar to 2529 Å³ at 10 bar, 2526 Å³ at 50 bar, and 2617 Å³ at 100 bar. At 100 bar, one water molecule slipped between F415 and H449, displacing the catalytic histidine side chain and thus opening the cavity to form a continuous water channel. The rotation of the side chain leads to a decreased distance between the H449-Nε and the (+)-menthyl-oxygen (non-preferred enantiomer) in the acyl enzyme intermediate, a factor determining the enantioselectivity of the lipase.

While the geometry of the preferred enantiomer is similar in all simulations, the geometry of the non-preferred enantiomer gets gradually more reactive. This observation correlates with the gradually decreasing enantioselectivity E.

Keywords: molecular dynamics, elevated pressure, stereoselectivity, *Candida rugosa* lipase, enantioselectivity, essential water

Introduction

Lipases (E.C. 3.1.1.3) stereoselectively catalyze hydrolysis as well as the reverse reaction, esterification and transesterification. The direction of the reaction can be influenced by the use of adequate solvent systems, aqueous or organic. Lipases are used for a wide variety of biotransformations and in preparative organic synthesis (Kazlauskas & Bornscheuer, 1998; Schmid & Verger, 1998). Natural substrates of lipases are esters of cholesterol or glycerol but lipases are commonly used in the synthesis of precursors for agrochemicals, pharmaceuticals or other synthetic targets (Cygler et al., 1994; Kazlauskas, 1994; Peters et al., 1996). The kinetic resolution of racemic secondary alcohols in organic solvent systems is a well studied application of lipases. Advantages of organic solvent systems are the high solubility of hydrophobic substrates or the ease of separation and reuse of the biocatalyst (Otero et al., 1988; Narang et al., 1990; Otero et al., 1995; Ivanov & Schneider, 1997). Even supercritical fluids have been used as solvent, thus facilitating downstream processing (Marty et al., 1992; Beckman et al., 1995; Ikushima, 1997). Intense research has been performed on the impact of various parameters on the stereoselectivity of lipases, such as immobilization, coating of lipases with surfactants, use of acid anhydrides as substrates or controlling stereoselectivity via the surface pressure of substrate monolayers (Rogalska et al., 1990; Ransac et al., 1991; Rogalska et al., 1991; Bianchi et al., 1993; Bornscheuer et al., 1993; Rogalska et al., 1993; Rogalska et al., 1993; Bornscheuer et al., 1995; Cygler et al., 1995; Kamiya et al., 1995; Stadler et al., 1995; Yang et al., 1996; Koteshwar & Fadnavis, 1997).

The effect of high pressure on protein dynamics and enzyme reaction has been studied to a lesser extent (Prokhorova et al., 1972; Greulich & Ludwig, 1976; Heremans, 1982; Chernyak et al., 1984; Kunugi et al., 1989; Suzdalev et al., 1991; Kunugi, 1992).

To understand the effect of pressure on structure, dynamics, and activity of enzymes, NMR (Akasaka et al., 1999; Li et al., 1999; Inoue et al., 2000; Kalbitzer et al., 2000) as well as molecular modeling studies (Kitchen et al., 1992; van Gunsteren & Brunne, 1993; Paci & Marchi, 1996; Floriano et al., 1998) have been carried out. NMR revealed that, in general, helical and loop regions show higher compressibility and volume fluctuation than ß-sheets (Akasaka et al., 1999; Kalbitzer et al., 2000). Molecular modeling studies have investigated the compressibility of proteins (Paci & Marchi, 1996; Kharakoz, 2000) or the pressure denaturation of proteins (Zipp & Kauzmann, 1973; Hummer et al., 1998). Only very small changes in average protein structure and internal energy are observed in molecular dynamics simulations due to the low compressibility of proteins (Kitchen et al., 1992; van Gunsteren & Brunne, 1993). Additionally, the compressibility of proteins depends on the activity of water (Kharakoz, 2000). The compressibility of water surrounding hydrophobic groups on the other hand seems to be much larger than that of water hydrating charged groups or even bulk water (Kitchen et al., 1992). Therefore, the effect of pressure on proteins or solvents, is best described, at least at pressures up to 100 bar, with rather local than global effects. Increasing the pressure above 500 bar, protein unfolding seems to be driven to a large extent by increasing the exposed hydrophobic surface area of the protein (Kitchen et al., 1992; Hummer et al., 1998; Li et al., 1999; Inoue et al., 2000). The energy of elastic deformation, induced by creating an internal cavity is the beginning of pressure denaturation. It can exceed the thermal motion energy (2.5 kJ/mole at room temperature) by an order of magnitude (Kharakoz, 2000).

The structure of several lipases have been well studied since 1990 (Cygler et al., 1993) with the structure of ***Candida rugosa*** lipase being available since 1993 (Grochulski et al., 1993; Grochulski et al., 1994). The α/β hydrolase fold is common to all lipases, and the catalytic triad consists of serine, aspartate or glutamate, and histidine (Ollis et al., 1992). The

catalytically active nucleophile, serine, is placed in the tip of a sharp loop, the nucleophilic elbow. While lipases have no general similarity, a consensus sequence common to all lipases is the amino acid sequence of the nucleophilic elbow; G-X-S-X-G-Sm, where Sm is a small residue.

Molecular modeling studies (Kazlauskas, 2000) on the stereoselectivity of lipases mostly perform conformational analysis (Uppenberg et al., 1995; Holmquist et al., 1996; Botta et al., 1997; Yagnik et al., 1997), the rational design of the active site (Scheib et al., 1998; Scheib et al., 1999; Manetti et al., 2000) or substrates (Stadler et al., 1995; Tafi et al., 2000) or energy based evaluation of enantioselectivity (Haeffner et al., 1998).

To date, no study has been reported providing a model for the observable pressure dependence of the enantioselectivity of *Candida rugosa* lipase. For the stereoselectivity of *Pseudomonas cepacia* lipase towards secondary alcohols, a quantitative model has been developed to predict the ranking of substrates by enantioselectivity (Schulz et al., 2000). According to this model, the distance between the catalytically active histidine and the substrate ester group of the non-preferred enantiomer correlates to the experimentally determined stereoselectivity. Schulz et al. found that low and high E-values correlate to small and large distances between the H286-Nε atom and substrate-O atom, respectively.

In this study, we report on the pressure dependence of *Candida rugosa* lipase-catalyzed enantioselectivity. *Candida rugosa* lipase displays a broad substrate spectrum (Kazlauskas & Bornscheuer, 1998) with the *Candida rugosa* lipase-catalyzed chiral resolution of (±)-menthol representing one of the most thoroughly studied reactions (Baratti et al., 1988; Salleh et al., 1993; Tseng et al., 1994; Kamiya & Goto, 1997; Furukawa & Kawakami, 1998). As a model reaction, esterification of racemic menthol with propionic acid anhydride in chloroform was investigated at 1, 10, 50, and 100 bar, respectively. A significant decrease in enantioselectivity of the lipase was observed for increasing pressure. In order to rationalize these

findings, we performed molecular dynamics simulations of the lipase in organic solvent (2289 molecules of chloroform) containing 244 essential water molecules and 17 sodium ions applying the same pressures as in the experiment.

Results

Biotransformation

The acylation of racemic menthol with propionic acid anhydride has been used to investigate the enantioselectivity of the ***Candida rugosa*** lipase (Figure 1). (±)-Menthol and the product, (±)-menthylpropionate were well resolved by gas chromatography (Figure 2). The retention times were 12.4 min for (+)- menthol, 12.6 min for (-)-menthol, 19.1 min for (-)-menthylpropionate, and 19.6 min for (+)-menthylpropionate. The experimentally observed enantioselectivity of ***Candida rugosa*** lipase, calculated using the peak areas for (+)- and (-)-menthol and (-)- and (+)-menthylpropionate, decreased from E=55 ± 1.5 (1 bar) to E=47 ± 2.1 (10 bar), E=37 ± 1.5 (50 bar), and E=9 ± 0.4 (100 bar) (Table 1 and Figure 3). The enantiomeric ratio of the products and substrates was analyzed at a conversion c between 30 % and 15 % after 24 hours (1 bar and 10 bar) and after 48 hours (50 bar and 100 bar) (Table 1). Increasing pressure leads to loss of activity; at 100 bar residual activity is 25 % of the activity at 1 bar. To account for the decrease in activity towards (±)-menthol at higher pressures in our experiment, we checked the loss in residual activity of the lipase after incubation at 1 bar and 100 bar using a pH-stat assay at ambient conditions. The activity of the commercially available lipase Amano AY (wild type) was 7.3 units/mg, whereas the lipase retained 6.4 units/mg (88 % of the wild type) after two days incubation in chloroform at 1 bar, and 6.8 Units/mg (93 % of the wild type) after two days incubation in chloroform at 100 bar. Thus, the loss in activity of the lipase towards (±)-menthol at higher pressures during our experiment is reversible and can be ascribed to the experimental conditions, as the residual activities of the lipase after incubation at 1 bar and 100 bar are nearly that of the wild type and show no irreversible denaturation of the lipase.
The water content was determined by loss on drying of 1 g of lipase Amano AY (LAYX03512) at 105 °C and 4 hours to 4.11 % [Koichi Suzuki: personal

communication]. We determined a water content of 6.3 % of the Amano AY lipase (LAYY04501025) preparation by Karl-Fischer titration.

Molecular dynamics simulations

Four molecular dynamics simulations of the ***Candida rugosa*** lipase were performed using chloroform as solvent. One molecular dynamics simulation of the ***Candida rugosa*** lipase was carried out using water as solvent. For the molecular dynamics simulation in water, the molecular weights of all the parts of our simulation assembly were 200 kDa for 11332 water molecules, 391 Da for 17 sodium ions and 57 kDa for the lipase. For the molecular dynamics simulations in chloroform, the molecular weights of all the parts of our simulation assembly were 274 kDa for 2289 chloroform molecules, 391 Da for 17 sodium ions, 57 kDa for the lipase and 4392 Da for 244 water molecules, with the 4392 Da for the water corresponding to 7.1 % of the overall molecular weight of our ***in silico*** lipase preparation. This matches well the experimentally determined 6.3 % water content of the lipase Amano AY. Pressures applied were 1 bar for the simulation in water and 1 bar, 10 bar, 50 bar, and 100 bar, respectively, for the simulations in chloroform. In the course of initial energy minimization, the total energy of the molecular dynamics simulation assembly reached a minimum at about −200,000 kJ/mol, however, after heating to 300 K it stabilized at about -100,000 kJ/mol after 1.3 ps of simulation. The size of the simulation assembly containing chloroform as solvent decreased during minimization and stabilized at all pressures at about 740 nm^3 after equilibration. The size of the simulation assembly containing water as solvent stabilized at about 830 nm^3 after equilibration (Figure 4).

Averaging the protein conformations

The protein structures obtained during the production phase of the molecular dynamics simulations were averaged for further analysis. The rms-values towards the crystal structure of all Cα-atoms of the simulated structures averaged over the last 50 ps of each simulation (production

phase) do not exceed 1.8 Å (Table 2). In case of the molecular dynamics simulation of *Candida rugosa* lipase in water, only the last 15 ps were used for averaging. Stability of the molecular dynamics simulations was validated by inspecting both energies and volume of the simulation assembly (Figure 4) and the radius of gyration (Figure 5A), the rms-values towards the crystal structure of all Cα-atoms in the protein (Figure 5B) and the rms-fluctuations during the production phase of the molecular dynamics simulations (Figure 7). In the course of the molecular dynamics simulations, we could observe strong changes in the radius of gyration and the rmsd values in the first 100 ps, whereas only slight changes are observable after 100 ps. The radius of gyration of the conformations in the course of the molecular dynamics simulations in water as well as in chloroform decreases in the first 100 ps, thereafter only slightly drifting towards larger values (Figure 5A). Similarly, the rms-values of the conformations in the course of the molecular dynamics simulations in water as well as in chloroform increase in the first 100 ps, thereafter only slightly drifting towards larger values (Figure 5B). In case of the molecular dynamics simulation of the *Candida rugosa* lipase in water, the radius of gyration begins to fluctuate after about 300 ps. This is due to flexible loops on the surface of the protein. Although the radius of gyration and the rmsd values of the molecular dynamics simulations show a slight drift towards larger values, the observable differences between the conformations at 1 bar, 10 bar, 50 bar, and 100 bar (Table 3) exceed the differences caused by the drift. Thus, we can conclude, that the molecular dynamics simulations at different pressures can be evaluated to search for a trend caused by increased pressure, even though equilibration was not yet completely reached.

Docking of (±)-menthylester into the simulated structures

The tetrahedral intermediate of (+)- and (-)- menthylester was docked into the averaged structures obtained from molecular dynamics simulations at

different pressures. For (+)-menthol, the non-preferred enantiomer, the atom-atom distance from H449-Nε to (+)-menthyl-alcohol-O ($d^{+}_{N\varepsilon\text{-}O}$) significantly decreases with pressure (Table 3 and Figure 10), whereas for (-)-menthol, the preferred enantiomer, the atom-atom distance from H449-Nε to (-)-menthyl-alcohol-O ($d^{-}_{N\varepsilon\text{-}O}$) only slightly decreases (Table 3 and Figure 10). The difference in the behavior of the atom-atom-distances ($\Delta d_{N\varepsilon\text{-}O} = d^{+}_{N\varepsilon\text{-}O} - d^{-}_{N\varepsilon\text{-}O}$) in our ***in silico*** experiment can be correlated to the ***in vitro*** experiment: large differences $\Delta d_{N\varepsilon\text{-}O}$ correspond to high enantioselectivity (at low pressure), small differences $\Delta d_{N\varepsilon\text{-}O}$ to low E-values (at high pressure) (Figure 6).

A second factor contributes to the decreased enantioselectivity at high pressures: the lone pair of the alcohol oxygen in (+)-menthol, the non-preferred enantiomer, gets oriented towards H449 with increasing pressure (Figure 10), thus facilitating the hydrogen transfer. The difference in the angle $(N\text{-}O)^{+}$ in our ***in silico*** experiment can be correlated to the ***in vitro*** experiment: large angles $(N\text{-}O)^{+}$ correspond to high enantioselectivity (at 1 bar and 10 bar), small angles $(N\text{-}O)^{+}$ to low E-values (at 50 bar and 100 bar) (Table 3).

Analysis of the averaged structures

Analyzing the crystal structure 1LPM revealed a cavity beginning at the surface of the lipase distinct from the substrate binding site, extending through the interior of the protein and ending near the catalytic histidine. The cavity is formed by side chains of E208, Q240, S241, G242, G336, D337, Q338, N339, D340, E341, G342, F345, Q387, G388, S389, F391, D392, K404, S407, A408, G411, D412, T416, L417, R419, A420, F434, L435, S436, K437, L502, M504, Y511, G513, K514, D515, N516, F517, and R518. It is filled with 6 water molecules (Figure 8A). In the molecular dynamics simulation with explicit water as solvent at 1 bar it is filled with 10

water molecules (Figure 8B). The number of water molecules in this cavity gradually increased with increasing pressure in our molecular dynamics simulations with crystal water and chloroform as solvent: 6 molecules in the simulation at 1 bar (Figure 8C), 10 molecules at 10 bar, 12 molecules at 50 bar, and 13 molecules at 100 bar (Figure 8D and Table 4). The side chain of H449 is gradually displaced from its initial position in the crystal structure as measured by the distance between F415-Cϕ and H449-Nε (Table 3). In the 100 bar simulation, a water molecule was observed between H449 and F415, thus turning aside the H449 sidechain (Figure 9 and Table 3). The cavity opens toward the active site and forms a continuous water channel (Figure 8D). The distance between H449-Nε and (+)-menthyl-O gets similar to the distance between H449-Nε and (-)-menthyl-O leading to converging reaction rates for (+)-menthol and (-)-menthol and, therefore, decreased enantioselectivity E (Figure 6 and Table 3). Each stereo view is in parallel eye mode.

Discussion

Biotransformation

The peaks for (+)- and (-)- menthol are not completely separated down to the baseline but still evaluable, whereas the corresponding peaks for (+)- and (-)- menthylpropionate are well separated. The standard deviation of the E-value was calculated using 6 samples.

With the experimentally determined water content of 6.3 % for the lipase preparation in the *in vitro* experiment and the water content of 7.1 % in the *in silico* experiment, we have set up an appropriate model of our *in vitro* experiment. In addition, the water content in the experiment will be further increased by the ongoing reaction as water will be produced as a by-product.

Molecular dynamics simulations

The first molecular dynamics simulation calculated was the simulation of *Candida rugosa* lipase with explicit water as solvent. The simulation time was 400 ps at 300 K and 1 bar pressure showing no change in volume of the simulation cell. The other molecular dynamics simulations were calculated with explicit chloroform as solvent, retaining the essential water molecules contained in the crystal structure of the *Candida rugosa* lipase, 1LPM. All molecular dynamics simulations were calculated with the inhibitor removed. There are several pdb-entries of the *Candida rugosa* lipase with different inhibitors in the active site: 1LPM with (1R)-menthylhexylphosphonate, 1LPN and 1LPO with dodecanesulfonate, 1LPP with hexadecanesulfonate and 1LPS with (1S)-menthylhexylphosphonate. Although containing different inhibitors, the backbone of the structure at the substrate binding site is not altered in these complexes. Given this rigidness of the backbone, Scheib et al. performed molecular dynamics simulations with the backbone fixed and could develop a model for the stereoselectivity of *Mucorales* lipases (Scheib et al., 1999). Thus,

simulating without bound inhibitor is a valid approach and should not interfere with our objectives.

Molecular dynamics simulations under a nanosecond are considered too short to be completely equilibrated (Daggett, 2000), but only few long timescale simulations of large proteins are reported yet (Aqvist, 1999; Daura et al., 1999; Alonso & Daggett, 2000; Radkiewicz & Brooks, 2000). After strong changes in the first 100 ps, the rms value against the crystal structure in all simulations reached a value of 1.5 Å - 1.8 Å after 400 ps of simulation. The difference in the atom-atom distance (Table 3) or the volume of the cavity (Table 4) in the averaged structures of our molecular dynamics simulations are larger than the differences caused by the small drift in rms values or radius of gyration (Figure 5A and Figure 5B), thus enabling us to further investigate the structural differences induced by applying pressure. Additionally, Alonso and Daggett (Alonso & Daggett, 2000) stated that the radius of gyration can be misleading as a reaction coordinate for unfolding/folding. For the pressure range of 1 bar to 100 bar, we would not expect a significant change in volume. Kitchen et al. found a compressibility of $\beta = 1.8 \times 10^{-2}$ kbar^{-1} (Kitchen et al., 1992). This would correspond to a change in volume of 0.18 %.

Analysis of the molecular dynamics simulations

For the enantioselectivity of ***Candida rugosa*** lipase-catalyzed esterification of (±)-menthol with propionic acid anhydride, a significant correlation could be observed between specific geometrical values of the averaged conformations obtained by molecular dynamics simulations and the experimentally determined E-values.

In this work, we propose a water channel which with increasing pressure is subsequently populated with water molecules. The water channel is limited by residues H449 and F415 in the core of the protein. Schulz et al. (Schulz et al., 2000) discussed for ***Pseudomonas cepacia*** lipase the atom-atom distance between H449-N and substrate ester-O to correlate to

stereoselectivity for the hydrolysis of secondary alcohol derivatives. While Schulz et al. correlate only the non-preferred enantiomer to the stereoselectivity, our model correlates the difference between the preferred and the non-preferred enantiomer to the enantioselectivity of the lipase. The lipase in the molecular dynamics simulations with chloroform as solvent gets more compact and rigid with increasing pressure, which resulted in a decreased radius of gyration compared to the molecular dynamics simulation in water as solvent (Figure 5A) and decreased fluctuations over the last 50 ps of each molecular dynamics simulation in chloroform as solvent (Figure 7). Kitchen and coworkers (Kitchen et al., 1992) found a bisection of the average mean square fluctuations in molecular dynamics simulations at 1 bar and 10 kbar, respectively. With the more rigid structure of the lipase, the activity towards (±)-menthol also decreases with increasing pressure (Table 1).

As observed, a channel in the structure of *Candida rugosa* lipase can bear an increasing number of water molecules with increasing pressure. Opening towards the surface of the lipase, its depth is limited by the active site H449 which plays a key role in the reported pressure dependent denaturation of *Candida rugosa* lipase. H449 in *Candida rugosa* lipase has been known for long to be involved in the enantioselectivity of the lipase (Cygler et al., 1994).

In 1987, for the first time Kauzman questioned the long established dogma that globular proteins are stabilized by a hydrophobic core (Kauzmann, 1987). In contrast to heat denaturation with a nonpolar molecule to be transferred from the nonpolar environment in the core of a protein towards its polar surface and, therefore, polar solvent, pressure denaturation can be understood as the transfer of water molecules into the protein (Hummer et al., 1998). Cavities in the protein structure are then filled with water molecules, destabilizing the protein and, eventually, unfolding it. This is accompanied by an initial increase in volume, followed by a decrease at pressures above 1 - 2 kbar.

Our work clearly shows the transfer of water molecules into the core of the protein. Thereby, a prebuilt cavity in the *Candida rugosa* lipase is enlarged, altering the enantioselectivity of the lipase. Limited by the pressure range of our investigation to pressures up to only 100 bar, we could not expect to observe everything related to what happens to the lipase or proteins at elevated pressures. However, obviously, our molecular dynamics simulations reflect the early stages of pressure induced protein denaturation. It is conceivable, that biochemical properties of proteins are altered before protein denaturation is completed.

Materials and methods

Biotransformations

The experimental setup for the chiral resolution of racemic (±)-menthol was as follows: 100 mg of (±)-menthol (640 µmol) and 100 mg of propionic acid anhydride (768 µmol) were mixed with 500 mg of Amano AY lipase in a 10 ml sample tube. The tube was sealed and subsequently filled with chloroform. For pressure regulation, an ISCO piston pump was used. The tube was placed in a temperature bath at 40°C and shaken at 300 rpm. Due to the enhanced pressures under which the experiments were carried out, it was not possible to take samples during the experiment. Therefore, each biotransformation was set up as described and stopped after 24 and 48 hours, respectively. The samples were analyzed by gas chromatography with the conversion rate held approximately constant at about 20 %. 0.5 µl aliquots of the experimentally obtained biotransformation assay were sampled by gas chromatography. The data were collected 6-fold. For each data set, the enantioselectivity, E, was calculated with the enantiomeric excess of the product, ee_p, and the enantiomeric excess of the substrate, ee_s, from the following equations (Chen et al., 1982; Chen et al., 1987):

$$E = \frac{\ln\left[(1-c)(1-ee_S)\right]}{\ln\left[(1-c)(1+ee_S)\right]} \qquad \text{with:} \qquad c = \frac{ee_P}{ee_P + ee_S}$$

The reaction of lipase-catalyzed esterification of racemic (±)-menthol with propionic acid anhydride can be described as follows (Figure 1):
In the main reaction, one molecule of (-)-menthol is esterified with propionic acid anhydride yielding (-)-menthylpropionate and propionic acid. However, if propionic acid is involved into the esterification of menthol, water can be formed as a byproduct. We did not apply the use of, e.g. molecular sieve to prevent the production of water.
Activity of the lipase was tested using a pH-stat assay. 10 mg of the lipase preparation were dissolved in 1 ml 20 mM phosphate buffer, pH 7. The pH-stat was filled with 20 ml of assay solution A (2 % gum arabicum, 200 ml

H_2O, 3 ml tributyrin) with the pH adjusted to pH 7.2. After addition of 100 µl of the dissolved lipase preparation, pH was titrated with 0.01 M NaOH. The water content of the commercially available lipase preparation of the *Candida rugosa* lipase was checked by Karl-Fischer titration.

Molecular dynamics simulation

The starting conformation for molecular dynamics simulations was the crystal structure of the open form of *Candida rugosa* lipase (pdb-entry 1LPM) (Cygler et al., 1994). Initially, the inhibitor (1R)-menthyl hexyl phosphonate was removed and the file type converted into GROMOS96 format using the program PROCS2. To fill free valences, the programs PROGCH (*Candida rugosa* lipase), PROGWH (essential H_2O) were used. Molecular topologies were calculated with PROGMT. Essential water molecules were treated as being part of the solute. In order to neutralize the system, the coordinates of 17 sodium ions were placed at positions with highest electrostatic potential as determined by the program PROION. PROBOX was used to fill a truncated octahedral box with chloroform molecules. The sizes of the initial solvent boxes were 824 nm^3 for the molecular dynamics simulation with water as solvent and 880 nm^3 for the molecular dynamics simulation with chloroform as solvent. With this complex, Steepest Descent energy minimization was performed 8 times for 3 steps, 7 times for 10 steps, and finally for 50 steps each with a time step of 2 fs. Subsequently, the simulation assembly was heated to 1 K, 5 K, 10 K, 50 K, 100 K, and 300 K for each 25 steps using PROMD. After an equilibration phase of 1 ps (500 steps), pressure coupling was set to 1 bar and the system was equilibrated for 100 ps. Here, temperature coupling was 0.1 ps, pressure coupling 0.5 ps with only the charged version of the GROMOS force field being used. Periodic boundary conditions (PBC) were applied to all simulations performed and the bond lengths were constrained applying the SHAKE algorithm. Nonbonded interactions were cut off after 8 Å and the nonbonded interaction pair list was updated every 10 simulation steps. Each

molecular dynamics simulation at elevated pressure was started using the configuration after 50 ps of the simulation at previous pressure. Therefore, the overall length of the molecular dynamics simulations at different pressures can be calculated as follows: 400 ps at 1 bar, 350 ps at 10 bar, 300 ps at 50 bar, and 250 ps at 100 bar respectively. However, only structures calculated during the production phase of molecular dynamics simulations (last 50 ps) were processed to generate an average structure of the molecule, however, without both essential water and chloroform solvent molecules. Into these averaged *Candida rugosa* lipase structures, the tetrahedral intermediate of (+)-/(-)-menthylester was manually docked and Steepest Descent minimization was applied.

The molecular dynamics simulations were carried out on a DEC Alpha 433au workstation using the program package GROMOS96 (van Gunsteren & Berendsen, 1987). Docking of the tetrahedral intermediate of (+)-/(-)-menthylester into of the resulting structures was performed manually applying SYBYL 6.5 (Tripos Inc., St.Louis, MO) on a SGI Indigo2 workstation.

Acknowledgments

We thank Erika Denzel at the Institute for Food Technology, University of Hohenheim, research group of Dipl. Ing. Nils Langer for determining the water content of the commercially available lipase preparation of the *Candida rugosa* lipase.

This work was supported by the German Federal Ministry of Education and Research (BMBF).

Especially, we thank the referees of our manuscript for their thorough reading and valuable comments.

References

Akasaka K, Li H, Yamada H, Li R, Thoresen T, Woodward C K. 1999. Pressure response of protein backbone structure. Pressure-induced amid 15n chemical shifts in BPTI. ***Protein Science 8***:1946-1953.

Alonso D O V, Daggett V. 2000. Staphylcoccal protein A: Unfolding pathways, unfolded states, and differences between the B and E domains. ***PNAS 97***:133-138.

Aqvist J. 1999. Long-range electrostatic effects on peptide folding. ***FEBS Letters 457***:414-418.

Baratti J, Buono G, Triantaphylides C, Langrand G. 1988. Enzymatic separation and resolution of nucleophiles: a predictive kinetic model. ***Biocatalysis 1***:231-248.

Beckman E J, Russell A J, Kamat S V. 1995. Enzyme Activity in Supercritical Fluids. ***Crit. Rev. Biotech. 15***:41-71.

Bianchi D, Battistel E, Bosetti A, Cesti P, Fekete Z. 1993. Effects of chemical modification on stereoselectivity of Pseudomonas cepacia lipase. ***Tetrahedron: Asymmetry 4***:777-782.

Bornscheuer U, Herar A, Capewell A, Wendel V, Kreye L, Scheper T, Voß E, Wünsche K, Meyer H H. 1995. Lipase-catalyzed kinetic resolution of 3-hydroxy esters: Optimization, batch, and continuous reactions. ***Ann. N. Y. Acad. Sci. 750***:215-221.

Bornscheuer U, Herar A, Kreye L, Wendel V, Capewell A, Meyer H H, Scheper T, Kolisis F N. 1993. Factors affecting the lipase catalyzed transesterification reactions of 3-hydroxy esters in organic solvents. ***Tetrahedron: Asymmetry 4***:1007-1016.

Botta M, Cernia E, Corelli F, Manetti F, Soro S. 1997. Probing the substrate specificity for lipases. II. Kinetic and modeling studies on the molecular recognition of 2-arylpropionic esters by Candida

rugosa and Rhizomucor miehei lipases. *Biochimica et Biophysica Acta 1337*:302-310.

Chen C S, Fujimoto Y, Girdaukas G, Sih C J. 1982. Quantitative analyses of biochemical kinetic resolutions of enantiomers. *J. Am. Chem. Soc. 104*:7294-7299.

Chen C S, Wu S H, Girdaukas G, Sih C J. 1987. Quantitative analyses of biochemical kinetic resolution of enantiomers. 2. Enzyme-catalyzed esterifications in water-organic solvent biphasic systems. *J. Am. Chem. Soc. 109*:2812-2817.

Chernyak V Y, Drachev V A, Nikolaeva N G, Chernyak B V. 1984. High-pressure enzyme kinetics. Lactate dehydrogenase in an optical cell that allows a reaction to be started under high pressure. *FEBS Letter 169*:97-100.

Cygler M, Grochulski P, Kazlauskas R J, Schrag J D, Bouthillier F, Rubin B, Serreqi A N, Gupta A K. 1994. A Structural Basis for the Chiral Preferences of Lipases. *J. Am. Chem. Soc. 116*:3180-3186.

Cygler M, Grochulski P, Schrag J D. 1995. Structural determinants defining common stereoselectivity of lipases toward secondary alcohols. *Can. J. Microbiol. 41*:289-96.

Cygler M, Schrag J D, Sussman J L, Harel M, Silman I, Gentry M K, Doctor B P. 1993. Relationship between sequence conservation and three-dimensional structure in a large family of esterases, lipases, and related proteins. *Protein Sci. 2*:366-382.

Daggett V. 2000. Long timescale simulations. *Current Opinion in Structural Biology 10*:160-164.

Daura X, van Gunsteren W F, Mark A E. 1999. Folding-Unfolding Thermodynamics of a b-Heptapeptide From Equilibrium Simulations. *Proteins 34*:269-280.

Floriano W B, Nascimento M A C, Domont G B, Goddard III W A. 1998. Effects of pressure on the structure of metmyoglobin: Molecular dynamics

predictions for pressure unfolding through a molten globule intermediate. *Protein Science 7*:2301-2313.

Furukawa S, Kawakami K. 1998. Characterization of *Candida rugosa* lipase entrapped into organically modified silicates in esterification of menthol with butyric acid. *J. Ferment. Bioeng. 85*:240-242.

Greulich K O, Ludwig H. 1976. High pressure enzyme kinetics of dextransucrase. *Biophys Chem 6*:87-94.

Grochulski P, Li Y, Schrag J D, Bouthillier F, Smith P, Harrison D, Rubin B, Cygler M. 1993. Insights into interfacial activation from an open structure of Candida rugosa lipase. *J. Biol. Chem. 268*:12843-12847.

Grochulski P, Li Y, Schrag J D, Cygler M. 1994. Two conformational states of Candida rugosa lipase. *Protein Sci. 3*:82-91.

Haeffner F, Norin T, Hult K. 1998. Molecular modeling of the enentioselectivity in lipase-catalyzed transesterification reactions. *Biophysical Journal 74*:1251-1262.

Heremans K. 1982. High pressure effects on proteins and other biomolecules. *Annu Rev Biophys Bioeng 11*:1-21.

Holmquist M, Haeffner F, Norin T, Hult K. 1996. A structural basis for enantioselective inhibition of Candida rugosa lipase by long-chain aliphatic alcohols. *Protein Science 5*:83-88.

Hummer G, Garde S, Garcia A E, Paulaitis M E. 1998. The pressure dependence of hydrophobic interactions is consistent with the observed pressure denaturation of proteins. *Proc. Natl. Acad. Sci. USA 95*:1552-1555.

Ikushima Y. 1997. Supercritical fluids: an interesting medium for chemical and biochemical processes. *Advances in colloid and interface science 71*:259-280.

Inoue K, Yamada H, Akasaka K, Herrmann C, Kremer W, Maurer T, Döker R, Kalbitzer H R. 2000. Pressure-induced local unfolding of the Ras binding domain of RalGDS. *Nature Structural Biology 7*:547-550.

Ivanov A E, Schneider M P. 1997. Methods for the immobilization of lipases and their use for ester synthesis. *J. Mol. Catal. B: Enzymatic 3*:303-309.

Kalbitzer H R, Görler A, Li H, Dubovskii P V, Hengstenberg W, Kowolik C, Yamada H, Akasaka K. 2000. 15N and 1H NMR study of histidine containing protein (HPr) from Staphylococcus carnosus at high pressure. *Protein Science 9*:693-703.

Kamiya N, Goto M. 1997. How is enzymatic selectivity of menthol esterification catalyzed by surfactant-coated lipase determined in organic media? *Biotechnol. Prog. 13*:488-492.

Kamiya N, Goto M, Nakashio F. 1995. Surfactant-Coated Lipase Suitable for the Enzymic Resolution of Menthol as a Biocatalyst in Organic Media. *Biotechnol. Prog. 11*:270-275.

Kauzmann W. 1987. Thermodynamics of unfolding. *Nature 325*:763-764.

Kazlauskas R J. 1994. Elucidating structure-mechanism relationships in lipases: prospects for predicting and enigneering catalytic properties. *TIBTECH 12*:464-472.

Kazlauskas R J. 2000. Molecular modeling and biocatalysis: explanations, predictions, limitations, and opportunities. *Curr Opin Chem Biol 4*:81-88.

Kazlauskas R J, Bornscheuer U T (1998). Biotransformations with Lipases. Biotransformations, VCH. **8:** 37-191.

Kharakoz D P. 2000. Protein Compressibility, Dynamics, and Pressure. *Biophysical Journal 79*:511-525.

Kitchen D B, Reed L H, Levy R M. 1992. Molecular dynamics simulation of solvated protein at high pressure. *Biochemistry 31*:10083-10093.

Koteshwar K, Fadnavis N W. 1997. Remote control of stereoselectivity: lipase catalyzed enantioselective esterification of racemic a-lipoic acid. *Tetrahedron:Asymmetry 8*:337-339.

Kunugi S. 1992. Enzyme reactions under high pressure and their applications. *Ann N Y Acad Sci 672*.

Kunugi S, Iwasaki K, Nomura A. 1989. Effect of pressure on plant endonuclease reactions. *Nucleic Acids Symp Ser 21*:133-134.

Li H, Yamada H, Akasaka K. 1999. Effect of pressure on the tertiary structure and dynamics of folded basic pancreatic trypsin inhibitor. *Biophysical Journal 77*:2801-2812.

Manetti F, Mileto D, Corelli F, Soro S, Palocci C, Cernia E, D'Acquarica I, Lotti M, Alberghina L, Botta M. 2000. Design and realization of a tailor-made enzyme to modify the molecular recognition of 2-arylpropionic esters by candida rugosa lipase. *Biochim Biophys Acta 1543*:146-158.

Marty A, Chulalaksananukul W, Willemot R M, Condorét J S. 1992. Kinetics of lipase-catalyzed esterification in supercritical carbon dioxide. *Biotechnol. Bioeng. 39*:273-280.

Narang J S, Barker S A, Gray C J. 1990. Immobilization of lipase from Candida cylindracea and its use in the synthesis of menthol esters by transesterification. *Enzyme Microb. Technol. 12*:800-807.

Ollis D L, Cheah E, Cygler M, Dijkstra B, Frolow F, Franken S M, Harel M, Remington S J, Silman I, Schrag J, et al. 1992. The α/β hydrolase fold. *Protein Engineering 5*:197-211.

Otero C, Ballesteros A, Guisan J M. 1988. Immobilization/stabilization of lipase from Candida rugosa. *Appl. Biochem. Biotechnol. 19*:163-175.

Otero C, Robledo L, Alcantara A R. 1995. Study of the stabilization of pure lipases: comparison of two different lipase-microgel derivatives. *J. Mol. Catal. B: Enzym. 1*:23-28.

Paci E, Marchi M. 1996. Intrinsic compressibility and volume compression in solvated proteins by molecular dynamics simulation at high pressure. *Proc. Natl. Acad. Sci. USA 93*:11609-11614.

Peters G H, van Aalten D M, Edholm O, Toxvaerd S, Bywater R. 1996. Dynamics of proteins in different solvent systems: analysis of essential motion in lipases. *Biophysical Journal 71*:2245-2255.

Prokhorova N I, El'ianov B S, Gonikberg M G, Khurgin I I. 1972. Effect of high pressure on the stereospecificity of enzyme reactions. *Biokhimiia 37*:742-747.

Radkiewicz J L, Brooks C L. 2000. Protein Dynamics in Enzymatic Catalysis: Exploration of Dihydrofolate Reductase. *J. Am. Chem. Soc. 122*:225-231.

Ransac S, Rogalska E, Gargouri Y, Deveer A M T J, Paltauf F, Gancet C, Dijkman R, De Haas G H, Verger R. 1991. Stereoselectivity of lipases. Hydrolysis of enantiomeric glyceride analogs by gastric and pancreatic lipases, a kinetic study using the monomolecular film technique. *GBF Monogr. 16*:117-122.

Rogalska E, Cudrey C, Ferrato F, Verger R. 1993. Stereoselective hydrolysis of triglycerides by animal and microbial lipases. *Chirality 5*:24-30.

Rogalska E, Ransac S, Verger R. 1990. Stereoselectivity of lipases. II. Stereoselective hydrolysis of triglycerides by gastric and pancreatic lipases. *J. Biol. Chem.*:20170-6.

Rogalska E, Ransac S, Verger R. 1991. Stereoselectivity of lipases. Stereoselective hydrolysis of triglycerides by gastric and pancreatic lipases. *GBF Monogr. (Lipases) 16*:135-9.

Rogalska E, Ransac S, Verger R. 1993. Controlling lipase stereoselectivity via the surface pressure. *J Biol Chem 15*:792-794.

Salleh A B, Basri M, Samah S M A, Razak C N A, Ampon K, Yunus W M Z W. 1993. Synthesis of oleic esters by lipase from Candida rugosa. *Proc. Malays. Biochem. Soc. Conf. Volume Date 1992, 17th*:21-24.

Scheib H, Pleiss J, Kovac A, Paltauf F, Schmid R D. 1999. Stereoselectivity of Mucorales lipases - a simple solution to a complex problem. *Prot. Sci. 8*:215-221.

Scheib H, Pleiss J, Stadler P, Kovac A, Potthoff A P, Haalck L, Spener F, Paltauf F, Schmid R D. 1998. Rational design of Rhizopus oryzae lipase with modified stereoselectivity toward triradylglycerols. *Protein Eng. 11*:675-682.

Schmid R D, Verger R. 1998. Lipases - interfacial enzymes with attractive applications. *Angew. Chem. Int. Ed. Engl. 37*:1608-1633.

Schulz T, Pleiss J, Schmid R D. 2000. Stereoselectivity of *Pseudomonas cepacia* lipase toward secondary alcohols: A quantitative model. *Protein Science 9*:1053-1062.

Stadler P, Kovac A, Haalck L, Spener F, Paltauf F. 1995. Stereoselectivity of microbial lipases . The substitution at position sn-2 of triacylglycerol analogs influences the stereoselectivity of different microbial lipases. *Eur. J. Biochem. 227*:335-343.

Suzdalev I P, Kurinov I V, Livshits L D, Krupianskii I F, Gol'danskii V I. 1991. The effect of high pressure of protein dynamics from Rayleigh scattering of Mossbauer irradiation data. *Dokl Akad Nauk SSSR 321*:842-845.

Tafi A, van Almsick A, Corelli F, Crusco M, Laumen K E, Schneider M P, Botta M. 2000. Computer simulations of enantioselective ester hydrolyses catalyzed by Pseudomonas cepacia lipase. *J Org Chem 65*:3659-3665.

Tseng G W M, Kazlauskas R J, Caron G. 1994. Kinetic resolutions concentrate the minor enantiomer and aid measurement of high enantiomeric purity. *Tetrahedron: Asymmetry 5*:83-92.

Uppenberg J, Ohrner N, Norin M, Hult K, Kleywegt G J, Patkar S, Waagen V, Anthonsen T, Jones T A. 1995. Crystallographic and molecular-modeling studies of lipase B from Candida antarctica reveal a stereospecificity pocket for secondary alcohols. *Biochemistry 34*:16838-16851.

van Gunsteren W F, Berendsen H J C 1987. *Groningen molecular simulation (GROMOS) Library Manual*. Groningen, biomos.

van Gunsteren W F, Brunne R M. 1993. Dynamical properties of bovine pancreatic trypsin inhibitor from a molecular dynamics simulation at 5000 atm. *FEBS 323*:215-217.

Yagnik A T, Littlechild J A, Turner N J. 1997. Molecular modelling studies of substrate binding to the lipase from Rhizomucor miehei. *J Comput Aided Mol Des 11*:256-264.

Yang H, Cao S, Han S P, Guo N N, Gao X G, Huang Z, Dong H, Zhang N, Yang T-S. 1996. Enhancing the stereoselectivity and activity of Candida species lipase in organic solvent by noncovalent enzyme modification. *Ann. N. Y. Acad. Sci. 799*:358-363.

Zipp A, Kauzmann W. 1973. Pressure denaturation of metmyoglobin. *Biochemistry 12*:4217-4227.

Tables

Table 1: Kinetic parameters of the transesterification reaction at different pressures. Standard deviations were calculated for each E-value with 6 independent measurements.

time [h]	pressure [bar]	conversion [%]	E-value
24	1	28	55 ± 1.5
24	10	20	47 ± 2.1
48	50	24	37 ± 1.5
48	100	15	9 ± 0.4

Table 2: rmsd values of all backbone Cα-atoms from the crystal structure of *Candida rugosa* lipase averaged over the last 50 ps of each simulation production phase. In case of molecular dynamics simulation with explicit water as solvent, the last 15 ps were used for averaging.

simulated pressure [bar]	rmsd [Å]
1	1.56
10	1.73
50	1.67
100	1.61
1 (water)	1.57

Table 3 Geometrical analysis of the averaged and energy minimized structures of *Candida rugosa* lipase containing the manually docked tetrahedral intermediate of (-)-and (+)-menthylester at increasing pressure. The angle $(N\text{-}O)^+$ was calculated using the scalar product of the vector from the His449-N□ to its hydrogen atom and the sum of the vectors of the neighbouring carbon atoms towards the (+)-menthyl ester oxygen atom. The distances listed in column 4 are taken from the averaged structure without docking of the transition state analogue.

	distance between His449-N□ and			angle
simulated pressure [bar]	(-)-menthyl-alcohol-O [Å]	(+)-menthyl-alcohol-O [Å]	Phe415-Cϕ [Å]	$(N\text{-}O)^+$ [°]
1	3.0	4.6	4.4	81.0
10	2.9	4.5	4.6	76.3
50	2.9	3.9	4.8	12.0
100	2.6	3.3	6.7	20.6

Table 4 Properties of the proposed water channel as analyzed in the averaged structures without docking. The volume of the cavity was estimated with the Cα-atoms of three amino acid pairs, R518/N339, L435/F391, and F517/G341, respectively. Only the water molecules were counted in the last configuration of each molecular dynamics simulation.
The volume was determined by measuring the distances between Arg518/Asn339, Leu435/Phe391 and Phe517/Glu341.

simulated pressure [bar]	volume [Å]	number of water molecules in the cavity
1	1864	6
10	2529	10
50	2526	12
100	2617	13

Figure legend

Figure 1 Kinetic resolution of racemic (±)-menthol with propionic acid anhydride.

Figure 2 Chromatogram of the biotransformation sample after 48 hours at 100 bar.

Figure 3 Experimentally determined pressure dependence of the enantioselectivity of *Candida rugosa* lipase towards the esterification of (±)-menthol with propionic acid anhydride. For conversion rates, c = 15 - 30 %, the enantioselectivity significantly decreased with increasing pressure. Standard deviations were calculated for each E-value for 6 independent measurements.

Figure 4 Volume of the simulation assembly during the molecular dynamics simulations in water and in chloroform. The conformation at 100 ps in water was taken as starting structure for the molecular dynamics simulation in chloroform at 1 bar. Starting structures for the simulation at elevated pressures were the configurations obtained after 50 ps of the simulation at previous pressure (depicted by the arrows).

1 bar/water 1 bar 10 bar 50 bar 100 bar

Figure 5A Radius of gyration during the molecular dynamics simulations in water at 1 bar and in chloroform at the different pressures. The

conformation at 100 ps in water was taken as starting structure for the molecular dynamics simulation in chloroform at 1 bar.

1 bar/water ——— 1 bar – – – 10 bar —·—· 50 bar ····· 100 bar

Figure 5B Rms during the molecular dynamics simulations in water at 1 bar and in chloroform at the different pressures. The conformation at 100 ps in water was taken as starting structure for the molecular dynamics simulation in chloroform at 1 bar.

1 bar/water ——— 1 bar – – – 10 bar —·—· 50 bar ····· 100 bar

Figure 6 Linear correlation between experimentally determined enantioselectivity E and the difference of distance between H449-Nε and menthyl-alcohol-O of the (+)- and (-)-enantiomer $\Delta d_{N\varepsilon\text{-}O}$. A correlation of $\rho_{X,Y}$ = 91.5 % was calculated for the pressure range of 1 bar to 100 bar by:

$$\rho_{X,Y} = \frac{\frac{1}{n}\sum_{i=1}^{n}(x_i - \mu_x)(y_i - \mu_y)}{\sigma_X \bullet \sigma_Y}$$ with μ_X, μ_Y : averages of x (E-values) and y ($\Delta d_{N\varepsilon\text{-}O}$) and σ_X, σ_Y standard deviations.

$\Delta d_{N\varepsilon\text{-}O} = d^{+}_{N\varepsilon\text{-}O} - d^{-}_{N\varepsilon\text{-}O}$

with $d^{+}_{N\varepsilon\text{-}O}$: distance between H449-Nε and (+)-menthyl-alcohol-O

$d^{-}_{N\varepsilon\text{-}O}$: distance between H449-Nε and (-)-menthyl-alcohol-O

The distances were measured according to figure 10.

Figure 7 Fluctuations averaged over all Cα-atoms in the last 50 ps of each molecular dynamics simulation at 1 bar, 10 bar, 50 bar, and 100 bar, respectively.

Figure 8 A Stereo view of the water channel in the crystal structure of *Candida rugosa* lipase, 1LPM. The channel is closed. The hydrogen atoms of the water molecules were calculated. B Stereo view of the water channel in the simulated structure of *Candida rugosa* lipase with explicit water as solvent at 1 bar. The conformation shown is a snapshot at 400 ps. The channel is closed. C Stereo view of the water channel in the simulated structure of the *Candida rugosa* lipase with explicit chloroform as solvent at 1 bar. The conformation shown is a snapshot at 400 ps. The channel is closed. D Stereo view of the water channel in the simulated structure of the *Candida rugosa* lipase with explicit chloroform as solvent at 100 bar. The conformation shown is a snapshot at 250 ps. The channel is open.

Figure 9 Pressure induced displacement of the H449 side chain in the active site of *Candida rugosa* lipase. The lipase structure was averaged over the last 50 ps of the 100 bar simulation with the coordinates of the 13 water molecules in the water channel taken from the snapshot at 250 ps (colored by atom: green (C), red (O), blue (N), white (H)). The (+)-menthylester was docked as tetrahedral intermediate to the averaged structure and energy minimized. For comparison, the crystal structure (1LPM) is shown in gray; it contains only 6 water molecules in the water channel.

Figure 10 The tetrahedral intermediate of (-)-menthylester (blue: isopropyl moiety oriented to the right side) and the (+)-menthylester (red: isopropyl moiety oriented to the left side) docked to the averaged structure of the molecular dynamics simulation at A) 1 bar, B) 10 bar, C) 50 bar, and D) 100 bar. The distance between H449-N□ and the alcohol oxygen is marked by arrows (blue: (-), red: (+)). With increasing pressure, the geometry of the

two enantiomers becomes similar and the lone pair of the alcohol oxygen gets oriented towards H449.

Figures

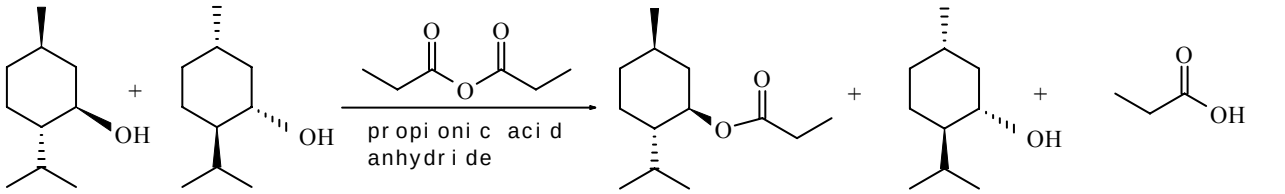

Figure 1

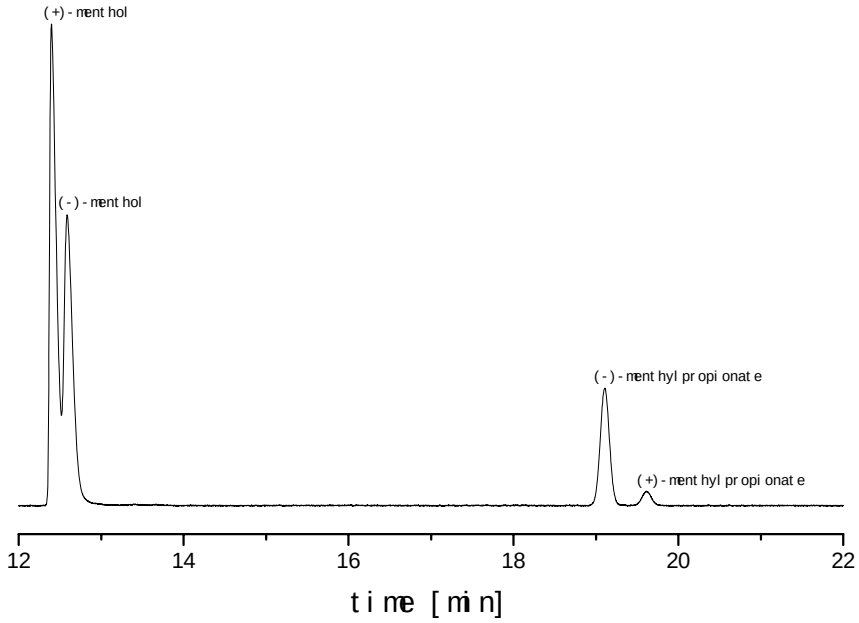

Figure 2

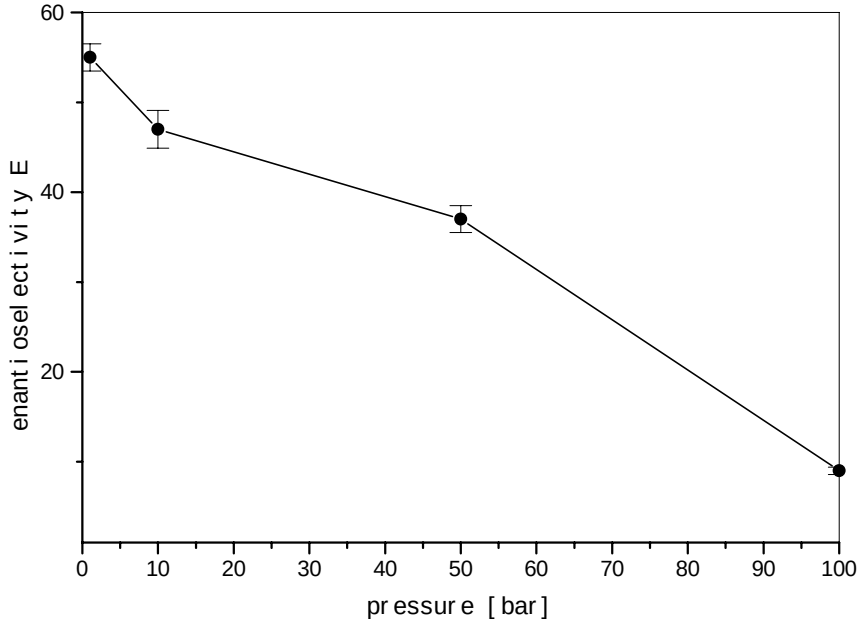

Figure 3

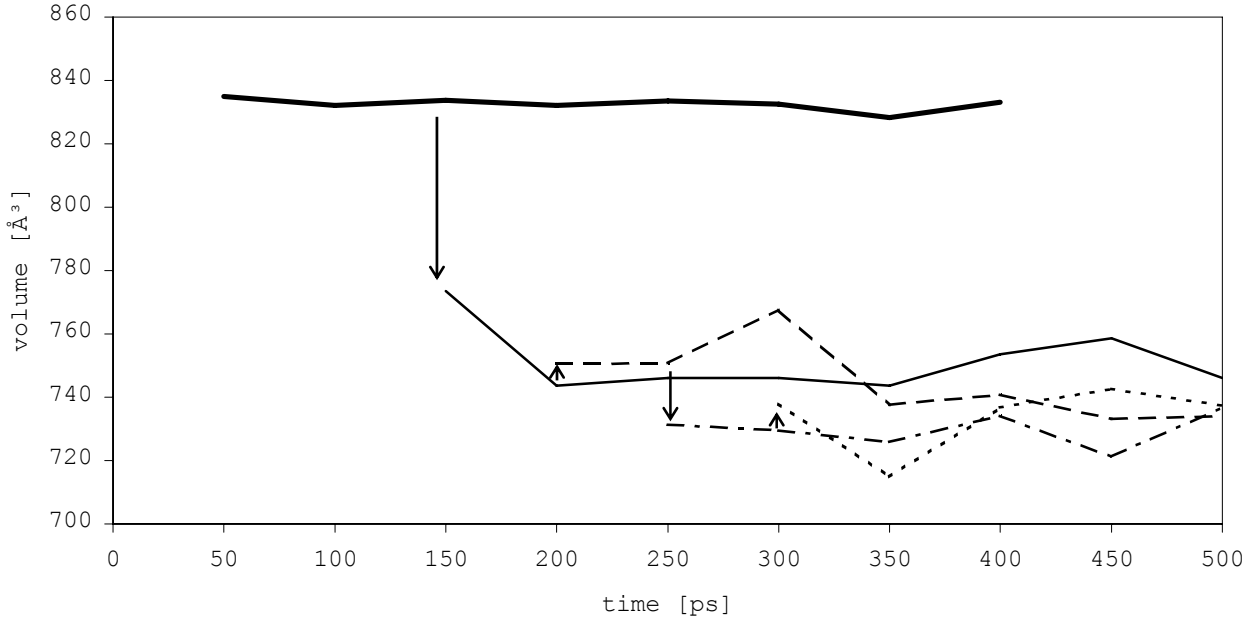

Figure 4

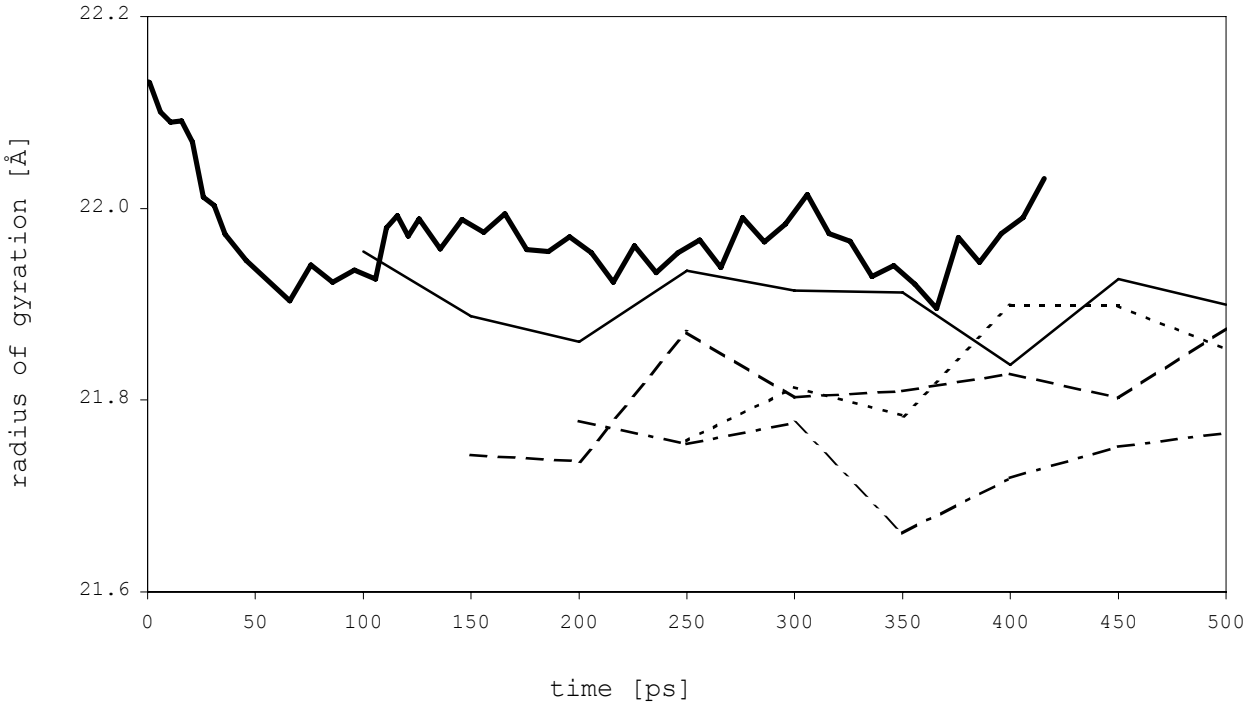

Figure 5A

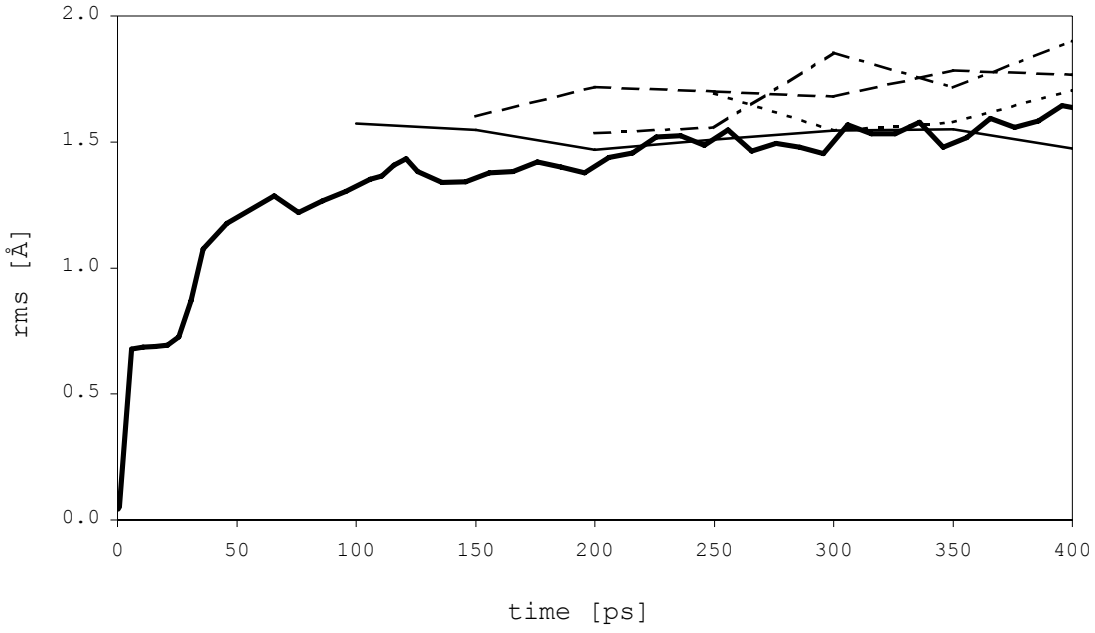

Figure 5B

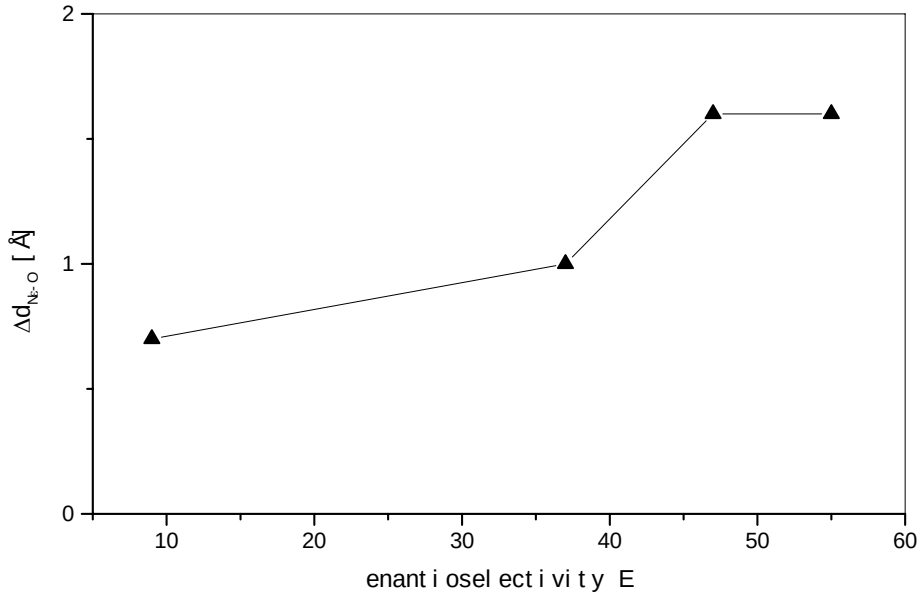

Figure 6

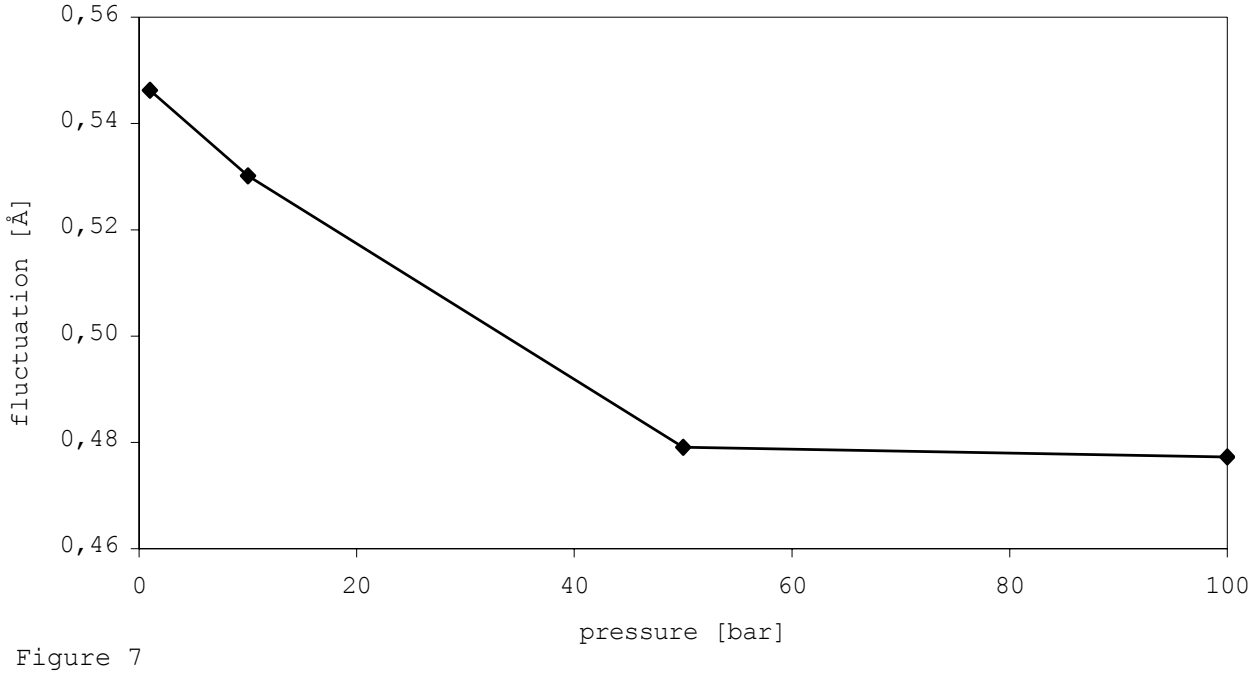

Figure 7

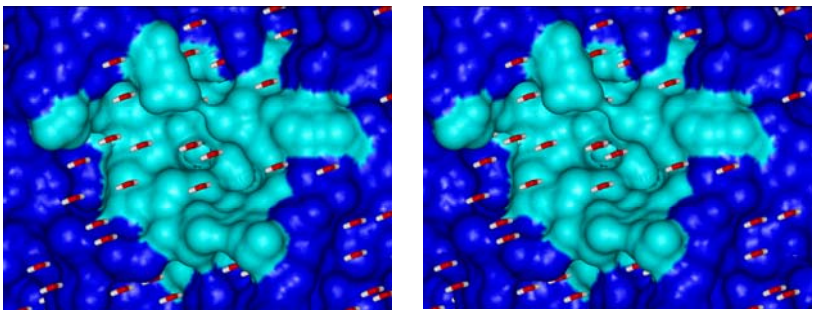

Figure 8A

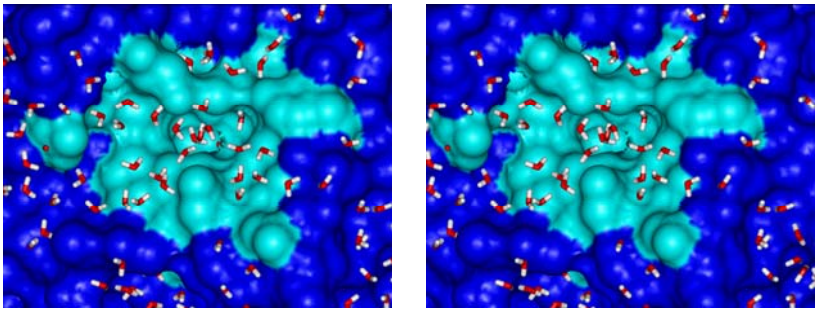

Figure 8B

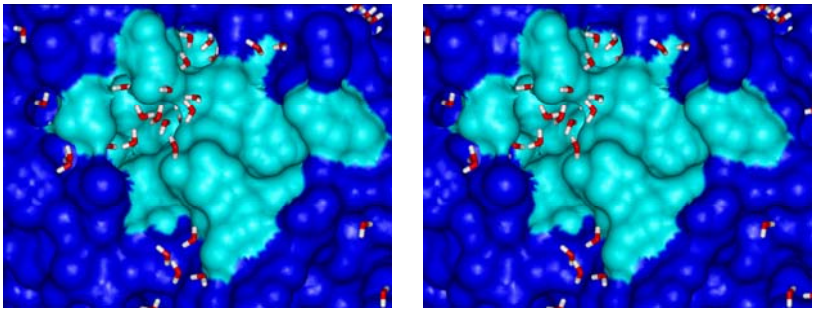

Figure 8C

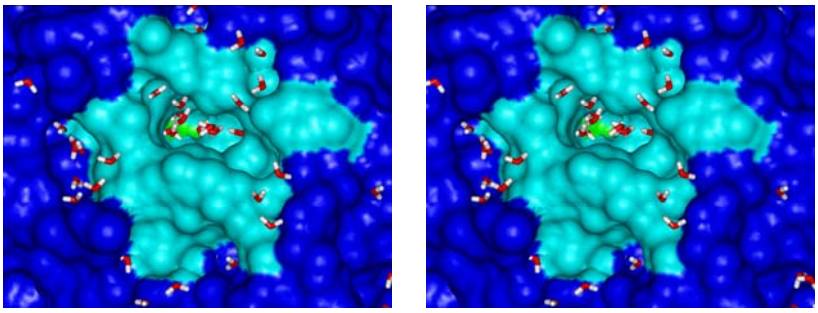

Figure 8D

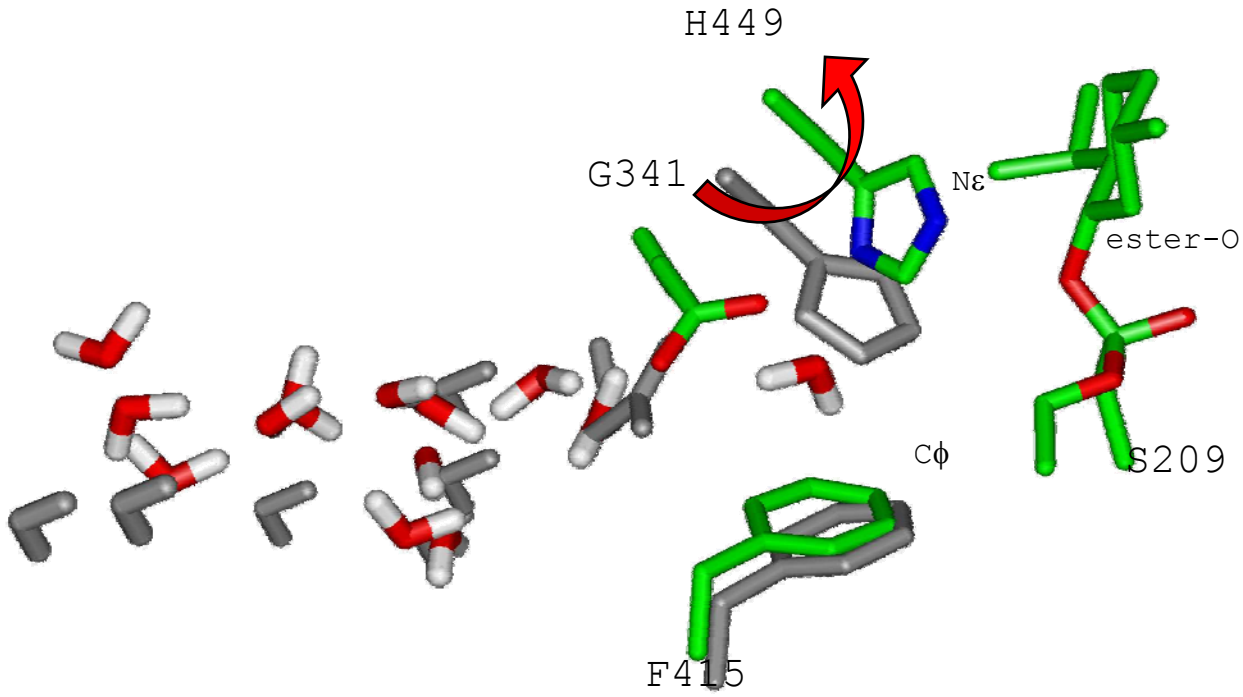

Figure 9

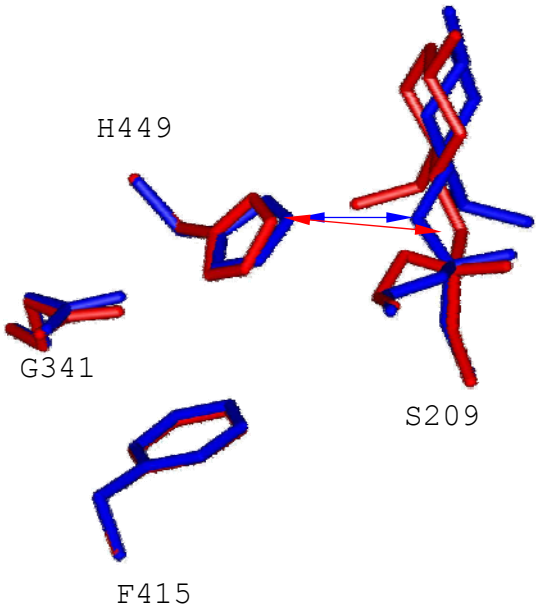

Figure 10 A

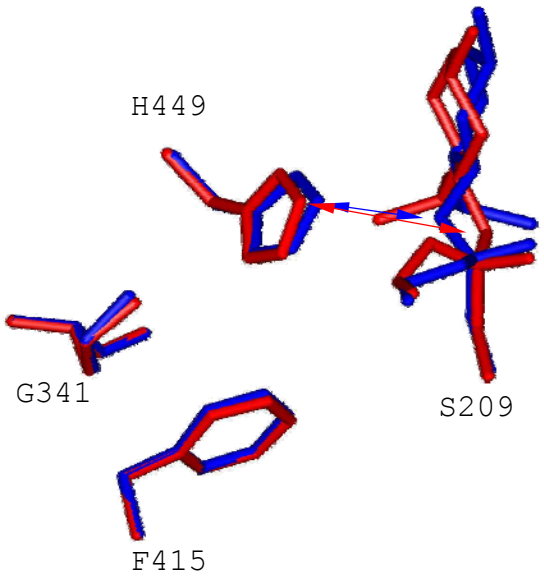

Figure 10 B

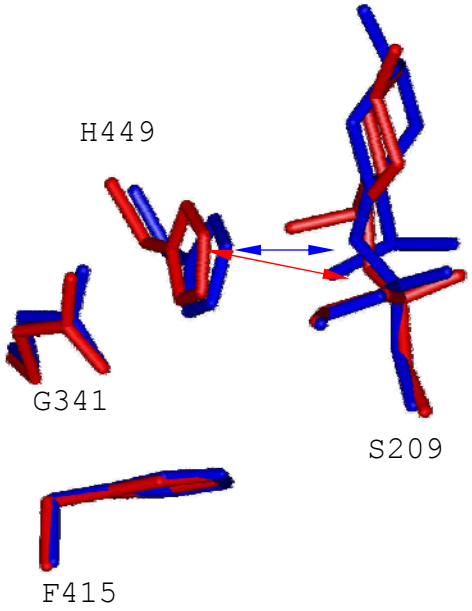

Figure 10 C

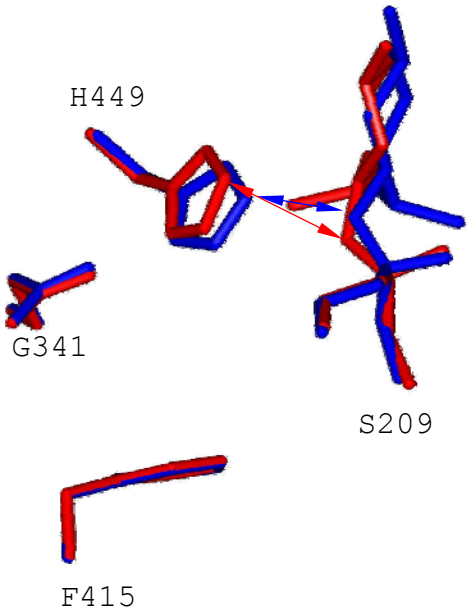

Figure 10 D